AGU PUBLICATIONS

JGR

Journal of Geophysical Research: Space Physics

RESEARCH ARTICLE

10.1002/2013JA019755

Key Points:

- There are sizable discrepancies between MHD and kinematic solar wind models
- Our MHD model needs ad hoc adjustments of the kinematic model boundary maps
- A time-dependent MHD tomography would provide more consistent boundary maps

Correspondence to:
T. K. Kim,
tae.kim@uah.edu

Citation:
Kim, T. K., N. V. Pogorelov, S. N. Borovikov, B. V. Jackson, H.-S. Yu, and M. Tokumaru (2014), MHD heliosphere with boundary conditions from a tomographic reconstruction using interplanetary scintillation data, *J. Geophys. Res. Space Physics*, *119*, 7981–7997, doi:10.1002/2013JA019755.

Received 2 JAN 2014
Accepted 2 SEP 2014
Accepted article online 8 SEP 2014
Published online 8 OCT 2014

MHD heliosphere with boundary conditions from a tomographic reconstruction using interplanetary scintillation data

T. K. Kim[1], N. V. Pogorelov[1], S. N. Borovikov[1], B. V. Jackson[2], H.-S. Yu[2], and M. Tokumaru[3]

[1]Center for Space Plasma and Aeronomic Research, University of Alabama in Huntsville, Huntsville, Alabama, USA,
[2]Center for Astrophysics and Space Sciences, University of California, San Diego, La Jolla, California, USA,
[3]Solar-Terrestrial Environment Laboratory, Nagoya University, Nagoya, Japan

Abstract Observations of interplanetary scintillation (IPS) provide a set of data that is used in estimating the solar wind parameters with reasonably good accuracy. Various tomography techniques have been developed to deconvolve the line-of-sight integration effects ingrained in observations of IPS to improve the accuracy of solar wind reconstructions. Among those, the time-dependent tomography developed at the University of California, San Diego (UCSD) is well known for its remarkable accuracy in reproducing the solar wind speed and density at Earth by iteratively fitting a kinematic solar wind model to observations of IPS and near-Earth spacecraft measurements. However, the kinematic model gradually breaks down as the distance from the Sun increases beyond the orbit of Earth. Therefore, it would be appropriate to use a more sophisticated model, such as a magnetohydrodynamics (MHD) model, to extend the kinematic solar wind reconstruction beyond the Earth's orbit and to the outer heliosphere. To test the suitability of this approach, we use boundary conditions provided by the UCSD time-dependent tomography to propagate the solar wind outward in a MHD model and compare the simulation results with in situ measurements and also with the corresponding kinematic solution. Interestingly, we find notable differences in proton radial velocity and number density at Earth and various locations in the inner heliosphere between the MHD results and both the in situ data and the kinematic solution. For example, at 1 AU, the MHD velocities are generally larger than the spacecraft data by up to 150 km s^{-1}, and the amplitude of density fluctuations is also markedly larger in the MHD solution. We show that the MHD model can deliver more reasonable results at Earth with an ad hoc adjustment of the inner boundary values. However, we conclude that the MHD model using the inner boundary conditions derived from kinematic simulations has little chance to match IPS and in situ data as well as the kinematic model does unless it too is iteratively fit to the observational data and measurements.

1. Introduction

Interplanetary space is permeated by charged particles streaming out from the Sun called the solar wind. Consisting of electrons, protons, alpha particles, and trace amounts of heavy ions, the solar wind convects the solar energy and magnetic field outward and balances the pressure from the partially ionized local interstellar medium (LISM) to form what is called the heliosphere. Since the source of the solar wind, the Sun, rotates and goes through periodic changes in its magnetic orientation, the three-dimensional (3-D) structure of the heliosphere also evolves over time. Furthermore, transient events such as coronal mass ejections (CMEs) often drive large-scale temporary disturbances in the solar wind structure and contribute to space weather phenomena. Such day-to-day random variations as well as long-term systematic changes in the solar wind plasma properties have been scrutinized with various types of in situ measurements and remote sensing observations to improve our understanding of the underlying physical processes.

While in situ measurements enable us to look into the solar wind directly, they are essentially single-point measurements with very limited spatial coverage. Moreover, the past and current in situ measurements of the interplanetary plasma are confined to a relatively small latitude band around the equatorial plane (±10°) with the exception of those provided by the Solar Wind Observations Over the Poles of the Sun instrument [*Bame et al.*, 1992] on board the Ulysses spacecraft, which ended its mission in 2009 as the only spacecraft to make solar wind measurements at nearly all heliographic latitudes (±80°) thus far. On the other hand, remote sensing observations (e.g., white light and radio wavelengths) allow us to probe vast expanses of the heliosphere that are currently inaccessible by spacecraft—especially the region between the Sun and Earth. Therefore, remote sensing observations can be particularly useful in providing inputs to numerical models of the solar wind, though interpretation and application of such observational data is generally not as straightforward as with in situ measurements. Moreover, the remote sensing observational data used in this study are mostly available beyond the Alfvén critical point [*Parker*, 1958] where the bulk flow speed of the background solar wind exceeds the Alfvén speed, so they bear an imprint of sophisticated and poorly understood physical phenomena occurring near the solar surface. The Alfvén critical point is considered to be located around 10–15 solar radii (R_s) at solar minimum and as high as 30 R_s at solar maximum by some estimates [*Zhao and Hoeksema*, 2010; *Goelzer et al.*, 2014].

Density irregularities in the interplanetary medium of typical scale length of a few hundred kilometers are responsible for scattering of radio waves from point-like celestial sources as they propagate through interplanetary space [*Hewish et al.*, 1964]. Ground observations of this phenomenon called interplanetary scintillation (IPS) have been particularly useful for studying the slowly varying, large-scale solar wind structure [*Coles et al.*, 1978; *Kojima and Kakinuma*, 1990; *Coles*, 1995; *Breen et al.*, 1997, 1998; *Bisi et al.*, 2007, 2010a; *Tokumaru et al.*, 2010, 2012; *Manoharan*, 2012; *Sokół et al.*, 2013]. Observations of IPS can be used to determine the solar wind velocity as a weighted average along each line of sight (LOS) between the observer and the radio source assuming that the density irregularities contributing to IPS are advected outward at the solar wind bulk flow speed. Since the largest amount of scattering is expected to occur around the point of closest approach (P-point) along the LOS to the Sun, it may be reasonable to assume the measured IPS speed to be the solar wind outflow speed at the P-point, though the development of various computer-assisted tomography methods has made this assumption largely obsolete. The techniques for analyzing the solar wind bulk speed have been well developed over the past several decades and shown to be qualitatively accurate even with such a simple approximation [*Watanabe and Kakinuma*, 1972; *Coles et al.*, 1978; *Coles and Kaufman*, 1978]. Nonetheless, IPS data are LOS-integrated values after all and thus require some tomographic procedure to properly unfold the LOS integration as described in the next section.

The IPS velocity can be measured from concurrent observations of radio sources by multiple stations [e.g., *Briggs et al.*, 1950; *Dennison and Hewish*, 1967; *Armstrong and Coles*, 1972; *Kakinuma et al.*, 1973; *Kojima*, 1979; *Bourgois et al.*, 1985; *Grall*, 1995; *Klinglesmith*, 1997; *Fallows et al.*, 2006, and *Breen et al.*, 2006] and also from single-station measurements [*Manoharan and Ananthakrishnan*, 1990]. In the case of multistation observations, the IPS velocity is estimated from the time lag for maximum cross correlation of the intensity spectra. However, more sophisticated methods involving full solar wind modeling of the two spectra and cross-correlation function can also be employed [e.g., *Coles*, 1996; *Klinglesmith*, 1997; *Breen et al.*, 2002; *Fallows et al.*, 2002, 2008, and *Bisi et al.*, 2007, 2010a]. For single-site measurements, the velocity is estimated by model fitting the power spectra. While the methods employed to derive the solar wind velocity can be somewhat different for single-site and multisite observations, a comparative analysis indicates that they produce results that complement each other [*Moran et al.*, 2000] (see also http://stesun5.stelab.nagoya-u.ac.jp/ips_nagoya.html for more recent studies).

Although single-station IPS systems are able to observe hundreds of sources per day, their range is inherently confined to the weak-scattering region, which falls closer to the Sun for higher observing frequencies [*Coles*, 1978]. This is important because in a weakly scattering medium, the observed scintillation can be approximated as a sum of contributions from a series of thin screens along the LOS. However, multistation IPS systems such as the Solar-Terrestrial Environment Laboratory (STEL) in Japan are capable of measuring solar wind velocities even in a strong-scattering region—albeit with lower accuracy than in a weak-scattering region [*Kojima et al.*, 2013].

The STEL IPS observatory consists of four radio telescopes scattered around Central Japan [*Kojima et al.*, 1982; *Kakinuma and Kojima*, 1984; *Kojima and Kakinuma*, 1986; *Tokumaru et al.*, 2011], of which only three are currently operational. Observing several tens of sources per day at the frequency of 327 MHz, the system currently provides daily measurements of the solar wind velocity and scintillation index for each LOS. Though observations of IPS do not directly provide the solar wind density, the amount of solar wind density turbulence can be inferred from what is called the g level, which is the ratio of the scintillation index to the mean value of scintillation index for a given source [e.g., *Gapper et al.*, 1982; *Jackson et al.*, 1998, and *Tokumaru et al.*, 2000a]. The g-level maps are especially useful for identifying interplanetary disturbances and analyzing their propagation [*Hewish and Bravo*, 1986; *Tappin*, 1987; *Tokumaru et al.*, 2000b, 2003a, 2003b, 2005, 2006, 2007]. Daily observations of IPS from STEL are also used to fit a 3-D heliospheric model to provide real-time solar wind forecasts at Earth (see http://ips.ucsd.edu/index_v_n.html for details). Furthermore, IPS-based time-dependent inner boundary values have recently been used to drive a 3-D multifluid model to simulate observations across the termination shock [*Kim et al.*, 2012, 2014].

This study focuses on heliospheric modeling with boundary values derived from STEL multistation observations of IPS [*Yu et al.*, 2012]. Since IPS data contain a bias (blurring) due to the LOS integration, a tomographic procedure is necessary to construct the time-varying boundary maps suitable for our 3-D magnetohydrodynamics (MHD) heliospheric model. Namely, the time-dependent tomography developed at University of California, San Diego (UCSD) [*Jackson et al.*, 1998, 2003, 2010, 2013; *Jackson and Hick*, 2004] is employed to obtain the inner boundary maps at a heliocentric distance that is sufficiently above the Alfvén critical point where implementation of the inner boundary values and modeling the solar wind flow are rather straightforward. In this study, our inner boundary is on a spherical surface at 0.25 AU from the Sun. We use the Multi-Scale Fluid-Kinetic Simulation Suite (MS-FLUKSS), which is a package of numerical codes that has been developed at the Department of Space Science and the Center for Space Plasma and Aeronomic Research at the University of Alabama in Huntsville (UAH) [*Pogorelov et al.*, 2009, 2010, 2013a; *Borovikov et al.*, 2009, 2013]. Originally designed to model the solar wind outflow in interplanetary space and the interaction between the solar wind and the LISM, MS-FLUKSS is arguably one of the most advanced numerical tools for modeling the physical processes occurring throughout the heliosphere [*Pogorelov et al.*, 2008, 2009, 2010, 2011, 2012a, 2012b, 2013a; *Kryukov et al.*, 2012]. Given realistic 3-D and time-dependent solar wind parameters, MS-FLUKSS is expected to deliver accurate outputs at Earth and other locations of interest in the global heliosphere.

In section 2, we describe the IPS tomography methods developed to reconstruct the 3-D inner heliosphere (i.e., within 3 AU), with a particular emphasis on the method that supplied the time-varying inner boundary conditions for our MHD model. In sections 3 and 4, we compare the solar wind parameters extracted from the MHD model along various spacecraft trajectories with the corresponding in situ data and also with the tomography output. Next, we attempt to match the MHD solution to spacecraft data by slightly altering the boundary values and analyze the results in section 5.

2. UCSD Tomographic Reconstruction of Inner Boundaries for the MS-FLUKSS Heliospheric MHD Model

Several types of tomography techniques have been developed to deconvolve the LOS integration effect intrinsic to observations of IPS. The corotating tomography, which was developed separately at STEL and at UCSD, combines a large number of lines of sight from an extended period (typically one or more Carrington rotations) to iteratively fit a quasi-stationary 3-D solar wind model [*Jackson et al.*, 1998; *Kojima et al.*, 1998; *Asai et al.*, 1998]. In the STEL version of the corotating tomography, an initial solar wind velocity distribution on a source surface at 2.5 R_s is radially extrapolated assuming constant speeds, and observations of IPS are simulated in the resulting 3-D solar wind model. After the difference between the simulated and observed IPS velocities is calculated, each LOS is ballistically traced back to the source surface where the initial velocity distribution is modified according to the velocity differences between simulated and observed IPS and appropriate weights along each LOS. The velocity distribution on the source surface is repeatedly altered until the 3-D solar wind model converges.

Hayashi et al. [2003] have subsequently developed the MHD-IPS tomography to provide 3-D reconstructions of the solar wind parameters such as velocity, number density, temperature, and magnetic field with a much improved time resolution of 1 day. Based on the STEL corotating tomography, the MHD-IPS tomography propagates the solar wind outward from a source surface at 50 R_s using a heliospheric MHD model to obtain a 3-D quasi steady state solution. The plasma parameters at the source surface are repeatedly modified until the model is best fit to IPS data in much the same way as in the STEL corotating tomography. Using the MHD-IPS tomography results as boundary conditions, *Hayashi et al.* [2011, 2012] and *Hayashi* [2012] have reconstructed the 3-D time-varying inner heliosphere for different periods. Despite the improved temporal resolution, the MHD-IPS tomography is limited to providing fuzzy snapshots of the 3-D solar wind structure because it uses IPS data for at least one full Carrington rotation (CR) centered around each given day to fit the steady state MHD model to observations of IPS. Thus, it is not suitable for analyzing transient, fast-evolving structures such as CMEs.

In contrast to the STEL version, the UCSD corotating tomography propagates the solar wind outward kinematically assuming conservation of the normalized proton number density and mass flux density [*Jackson et al.*, 1998]. This is a reasonable assumption for plasma propagation out to 1 AU that is consistent with the findings of the lineup study with the Helios 1 and 2 spacecraft [*Schwenn*, 1990]. Therefore, it starts with distributions of velocity and density on a source surface at 15 R_s and fits its 3-D solar wind model to IPS data in a manner similar to the STEL version. However, since the kinematic model accounts for density in addition to velocity, each iteration involves modification of density distribution on the source surface as well. *Jackson et al.* [1998] provide a detailed flow chart of this tomography program.

To improve upon the UCSD version of the corotating tomography, which is best suited for analyzing the long-term variations of the large-scale, slowly evolving heliosphere, *Jackson et al.* [2003, 2010, 2013] have developed the time-dependent tomography. By using a smaller number of LOS from each day's observation—typically around 30 for STEL IPS data—they have managed to boost the temporal resolution to 1 day, but the spatial resolution has decreased as a result. With STEL IPS data, the time-dependent tomography typically employs a $20° \times 20°$ spatial resolution at the source surface at 15 R_s, which is markedly lower than the $5° \times 5°$ resolution for the UCSD corotating tomography. However, the improved temporal resolution has enabled the UCSD tomography to reproduce the solar wind speed and density at Earth more accurately [e.g., *Jackson et al.*, 2003] and to analyze transient structures like ICMEs [e.g., *Bisi et al.*, 2008, 2009a, 2009b, 2010b, 2010c], making it a potentially powerful tool for solar wind forecasting. The UCSD group has also combined IPS velocity data with high-resolution heliospheric density imaging data from the Solar Mass Ejection Imager (SMEI) instrument [*Eyles et al.*, 2003; *Jackson et al.*, 2004] on board the Coriolis satellite [e.g., *Jackson et al.*, 2006, 2007a; *Bisi et al.*, 2008], but SMEI was deactivated in 2011. A detailed review of the UCSD tomography is available from *Jackson et al.* [2011].

With the inclusion of in situ measurements by near-Earth spacecraft—such as Advanced Composition Explorer (ACE), Solar and Heliospheric Observatory, and Wind—to further constrain the solar wind parameters on the source surface, the UCSD time-dependent tomography is able to reproduce the daily fluctuations in solar wind radial velocity and density at Earth with improved accuracy [*Jackson et al.*, 2010, 2013]. This brings to our attention the possibility of using the kinematic inner boundary values as an input to a more sophisticated solar wind model such as a heliospheric MHD model as previously attempted by *Bisi et al.* [2008]. Assuming that the kinematic solar wind model best fit to IPS data and near-Earth spacecraft measurements provides a fairly accurate representation of the solar wind within 1 AU, we expect that a MHD model, which is generally regarded as more advanced and realistic than a kinematic model, should produce comparable results at Earth while improving the solar wind reconstruction everywhere in the computational region, including distances larger than 1 AU. In that case, we may propagate the solar wind completely out to the LISM for a truly global reconstruction of the 3-D heliosphere.

The MHD solar wind model used by the UAH group and the kinematic solar wind model used in the UCSD time-dependent tomography differ mainly in the following ways. First, the solar wind velocity is assumed to be strictly radial in the kinematic model, and it does not change with heliocentric distance except to conserve mass and mass flux as solar wind structures of different speeds interact with each other in interplanetary space. On the other hand, we expect a moderate acceleration of the supersonic, super-Alfvénic solar wind due to polytropic expansion in the MHD model. Second, stream interaction dynamics (and the resulting changes in the solar wind parameters) are much more complex in the MHD model than in the kinematic model, so it is interesting to see how the 3-D solar wind reconstruction by the MHD model would compare with in situ measurements and the kinematic model, provided that the models employ the same boundary values. Therefore, we investigate the model differences by comparing the solutions at various heliocentric distances obtained with the same IPS-derived time-dependent inner boundary conditions for CRs 2114–2115 (26 August to 19 October 2011) and 2058–2063 (21 June to 1 December 2007). The former period is of particular interest because our previous MHD analysis concerning the same time period yielded conflicting results possibly due to some unforeseen errors [*Kim et al.*, 2014]. The latter period is ideal for modeling the ambient solar wind because it was an extremely quiet period largely devoid of transient structures. Moreover, off-ecliptic measurements are available from Ulysses during this period, thereby allowing us to analyze the models at various heliographic latitudes.

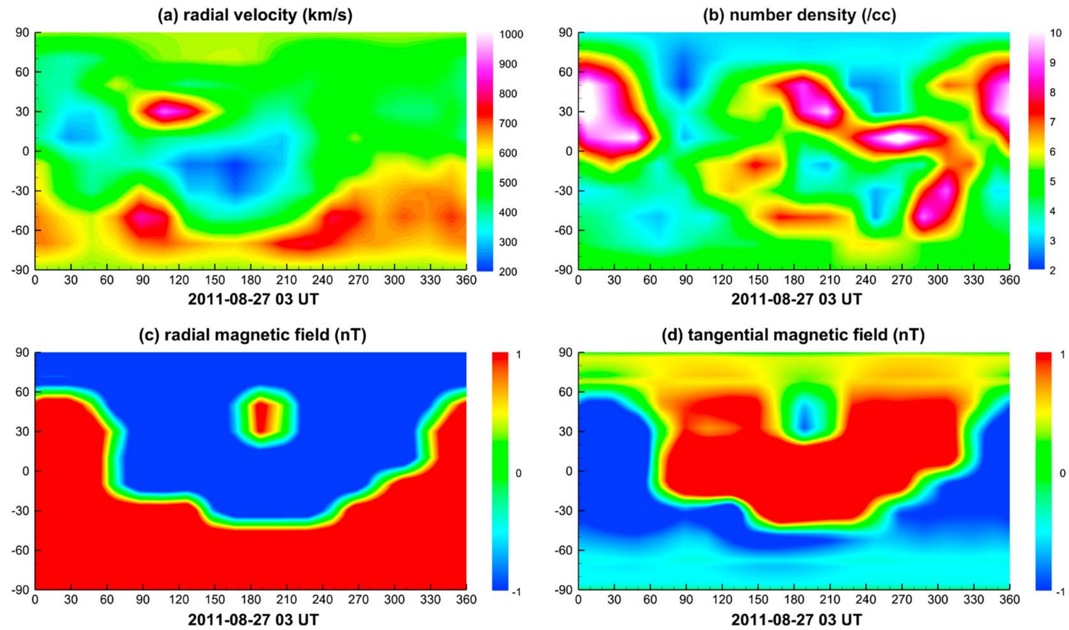

Figure 1. Boundary values for 27 August 2011 at 0.25 AU consisting of the proton (a) radial velocity (km s^{-1}), (b) number density (cm^{-3}), (c) radial, and (d) tangential components of magnetic field (nT). The number density and radial magnetic field component are scaled to 1 AU assuming a R^{-2} dependence, while the tangential magnetic field component is scaled by R^{-1}.

In a recent study [*Kim et al.*, 2014], we used boundary values from the UCSD kinematic model fit to daily STEL-IPS data and in situ measurements by the Solar Wind Experiment (SWE) instrument [*Ogilvie et al.*, 1995] on board the Wind spacecraft. This is reasonable because we compare our model with OMNI data, which consist mostly of Wind and ACE Level 2 data. However, while the kinematic velocity and density values at Earth matched the OMNI data very closely, we noticed a large discrepancy between the MHD results and OMNI data at Earth that were most likely caused by differences in some of the key aspects of the two models, i.e., the solar wind acceleration in polytropic expansion from 0.25 to 1 AU in the MHD model and the lack of such in the kinematic model and the mechanisms in which the solar wind density and velocity change as a result of stream interactions. It is also possible that some of the sharp peaks and troughs may have been smoothed out unexpectedly after multiple steps of interpolation (both spatial and temporal) at the boundary surface, therefore adding to the observed model differences at Earth.

As mentioned earlier, the time-dependent tomography employs a 20° × 20° resolution in longitude and latitude with a 1 day cadence for STEL IPS data, but the tomography program can interpolate the 3-D solution internally to output the solution at higher spatial and temporal resolution. In previous studies, we used kinematic boundary data given in such a way at 0.25 AU with a 5° × 5° resolution and a 24 h cadence, which we further interpolated to approximately 1.4° × 0.7° before feeding into MS-FLUKSS. Thus, it is possible for some of the sharp features at the boundary to have experienced some flattening in the combined process. To investigate how much (if at all) this "flattening" of the peak values at the boundary contributes to the difference between the model outputs at Earth, we boost the spatial resolution of the kinematic boundary maps from 5° × 5° to 1.4° × 0.7° and output the values at the exact coordinates used by MS-FLUKSS to minimize the number of interpolations performed at the boundary. We also push the temporal resolution of the boundary values from 1 day to 6 h.

3. Simulation Results for CRs 2114–2115 (26 August to 19 October 2011)

In this section, we examine the MHD solar wind model using the higher-resolution kinematic boundary values fit to STEL-IPS and Wind-SWE data for CRs 2114–2115. While the kinematic model used in the time-dependent tomography only requires the number density and speed to propagate the solar wind out to 1 AU and beyond, the MHD model needs additional parameters such as magnetic field and temperature.

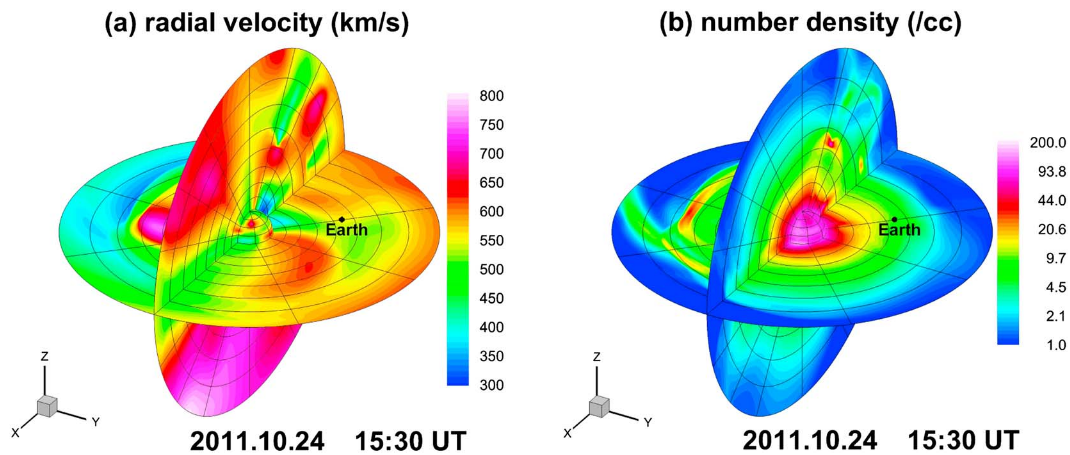

Figure 2. (a) Radial velocity (km s^{-1}) and (b) proton number density (cm^{-3}) on 24 October 2011 shown in the equatorial and meridional planes between 0.25 and 2 AU. The approximate position of Earth is shown projected onto the equatorial plane.

To obtain the magnetic field components at the boundary, we extrapolate the magnetic field from the solar surface to 15 R_s using the current sheet source surface model [*Zhao and Hoeksema*, 1995] and then to 0.25 AU by convecting them outward using a kinematic model with tomograhically derived global velocities [*Dunn et al.*, 2005]. At the boundary, we assume that the flow is entirely radial and the magnetic field has zero latitudinal component. Furthermore, we calculate the proton temperature from empirical correlations with the flow speed determined from Ulysses spacecraft measurements for solar cycle 23 [*Ebert et al.*, 2009; *Pogorelov et al.*, 2013b]. Figure 1 shows two-dimensional maps of the proton radial velocity, number density, and the radial and tangential components of magnetic field at 0.25 AU for 27 August 2011 reconstructed by the tomography using the STEL IPS data and the Wilcox Solar Observatory magnetograms.

In our heliospheric MHD model, the solar wind is treated as a single stream of protons with a set of physical properties such as velocity, density, magnetic field, and temperature. We solve a set of ideal MHD equations in a spherical coordinate system with four levels of adaptive mesh refinement in the Chombo framework [*Kryukov et al.*, 2006a, 2006b, 2008; *Borovikov et al.*, 2009]. The original boundary data given by the time-dependent tomography are in heliographic inertial coordinates and have a 256 × 256 resolution in latitude and longitude, with a 6 h cadence. The typical time step in our simulation is about 3 orders of magnitude smaller than the 6 h cadence, so we linearly interpolate between each frame in a corotating coordinate system to approximate the boundary values at each time step during the MHD simulation. Since we perform our calculations in an inertial coordinate system, the interpolated boundary frames are shifted appropriately in the process.

In Figure 2, we show the MHD proton radial velocity and number density on 24 October 2011 in the equatorial and meridional planes between the heliocentric distances of 0.25 and 2 AU. Interestingly, *Jian et al.* [2013] have identified a number of stream interaction regions (SIRs), as well as a few ICMEs, at 1 AU from the plasma measurements by ACE and the Solar Terrestrial Relations Observatory (STEREO) spacecraft during the simulated period (see http://www-ssc.igpp.ucla.edu/~jlan/ACE/Level3/SIR_List_from_Lan_Jian.pdf, http://www-ssc.igpp.ucla.edu/~jlan/ACE/Level3/ICME_List_from_Lan_Jian.pdf, http://www-ssc.igpp.ucla.edu/~jlan/STEREO/Level3/STEREO_Level3_SIR.pdf, and http://www-ssc.igpp.ucla.edu/~jlan/STEREO/Level3/STEREO_Level3_ICME.pdf for the full lists). Since the MHD radial velocity was excessively large compared to the OMNI and kinematic velocities in the previous simulation around the ICME arrival on this particular day, we reexamine this period by comparing the MHD solution obtained with high-resolution boundary values with that of the previous MHD solution.

3.1. Comparisons at Earth

We extract the simulated plasma parameters at Earth at 6 h intervals for comparison with OMNI 1 h averaged data and the kinematic output. In particular, we show comparisons of the proton radial velocity and number density here. Additionally, we compare the model plasma parameters to in situ measurements by

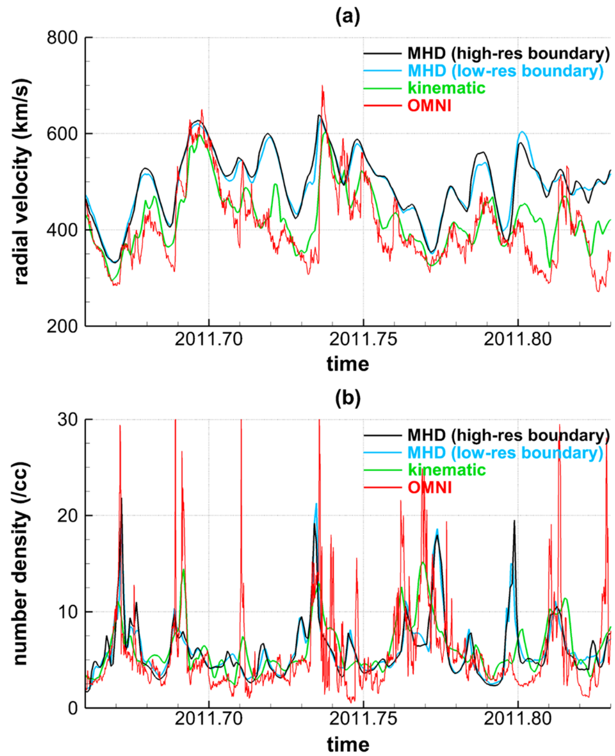

Figure 3. (a) Radial velocity (km s^{-1}) and (b) proton number density (cm^{-3}) at Earth for CRs 2114–2115 (26 August to 19 October 2011). The MHD solutions (black and light blue) are shown together with OMNI 1 h averages (red) and the kinematic solution (green).

the Plasma and Suprathermal Ion Composition instruments [*Galvin et al.*, 2008] on board the twin STEREO spacecraft. Orbiting the Sun at approximately 1 AU, STEREO-A leads and STEREO-B trails the Earth by 90° during this period.

Figure 3 provides the radial velocity and number density comparisons at Earth. The MHD solutions from the high-resolution boundary values are shown in blue, whereas the previous results are shown in orange. We have also included the OMNI 1 h average data and the corresponding kinematic solution for reference, which are shown in red and green, respectively. For the most part, the difference between the MHD results is negligibly small throughout the entire period except around 14 October 2011 (2011.79) and 20 October 2011 (2011.80) when the velocity differences are as large as 20–30 km s^{-1}. Though not negligible, these differences are still fairly small compared to the 100–150 km s^{-1} differences between the MHD model and the reference (in situ and kinematic) velocities. Hence, the smoothing of the peaks and troughs at the inner boundary appears to be only a minor factor for structures with sharp velocity and density gradients and is mostly insignificant for the ambient solar wind.

Now we turn our attention back to the large velocity differences seen between the MHD model and the reference values. Though not shown in this paper, we note the relative lack of well-defined SIRs at 1 AU in the ecliptic plane in the initial steady state solution. However, SIRs start developing within 1 AU shortly after we begin feeding the time-varying boundary values into the code. In Figure 3a, the velocity difference is initially small (20–30 km s^{-1}), but once we encounter a compression region ahead of a possible SIR around 2011.67, the difference grows much larger. The same can be said about the proton number density shown in Figure 3b. It appears that in many of the compression regions, which may also be associated with the presence of CMEs and their interaction with the background solar wind during this period, the density fluctuations are generally much larger in the MHD model than in the kinematic model.

3.2. Comparisons at STEREO

In Figure 4, we have provided additional comparisons of proton radial velocity and density at STEREO-A and STEREO-B. Unlike at Earth, the kinematic model poorly matches the in situ measurements at both locations. At STEREO-A, the fluctuations in the kinematic velocity and density and the timing of those fluctuations do not coincide with spacecraft measurements at all. The same can be said about the magnitude of kinematic velocity and density fluctuations at STEREO-B. However, the timing of the fluctuations appears to match somewhat better with that in the spacecraft measurements.

On the other hand, the MHD results follow the kinematic solution somewhat more closely at STEREO-A, where the MHD velocity is no larger than the kinematic velocity by 100 km s^{-1} at any time and stays mostly within less than 50 km s^{-1} as seen in Figure 4a. At STEREO-B, however, the radial velocity difference between the two models sometimes exceeds 100 km s^{-1}, which is similar to the model differences at Earth.

Overall, the MHD velocities are considerably larger at 1 AU compared to in situ data and kinematic values. Only a minor portion of these velocity differences can be attributed to acceleration in the polytropic

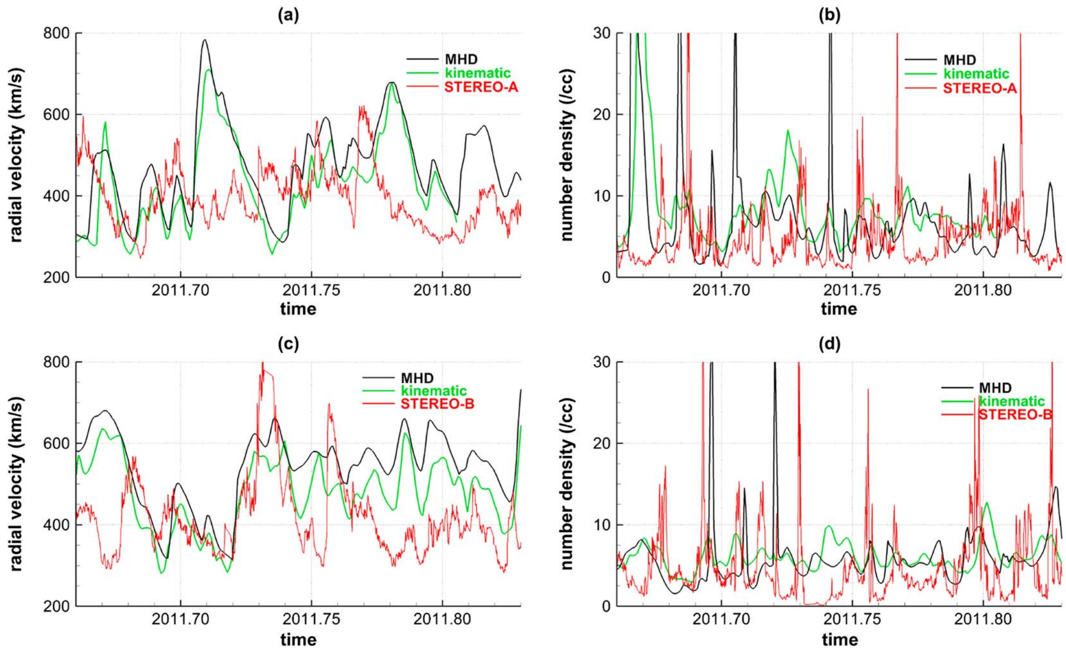

Figure 4. (a and c) Radial velocity (km s^{-1}) and (b and d) proton number density (cm^{-3}) at STEREO-A and STEREO-B for CRs 2114–2115 (26 August to 19 October 2011). One hour averages of STEREO data are shown as reference. The MHD solution is shown in black, while in situ data and kinematic values are shown in red and green, respectively.

expansion of the solar wind from 0.25 to 1 AU in the MHD model (see Appendix A). Without streams of different speeds interacting with each other or with transient structures, a moderate acceleration (up to 50–60 km s^{-1}) is expected from 0.25 to 1 AU in a MHD model. In reality, however, this polytropic acceleration does not necessarily require the solar wind speed to increase with distance because other physical processes (e.g., stream interactions and time-dependent boundary conditions) can cause the higher-speed wind to slow down while further accelerating the lower speed wind. We note that a number of SIRs and CMEs sweep through 1 AU during this period and are likely responsible for some of the large discrepancies seen in the MHD solution.

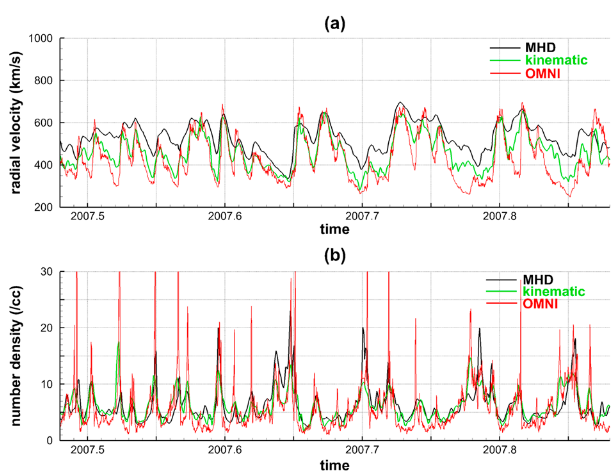

Figure 5. (a) Radial velocity (km s^{-1}) and (b) proton number density (cm^{-3}) at Earth for CRs 2058–2063 (21 June to 1 December 2007). One hour averages of in situ measurements are shown as reference. The MHD solution is shown in black, while the in situ data and kinematic values are shown in red and green, respectively.

4. MHD Simulation Results for CRs 2058–2063 (21 June to 1 December 2007)

CRs 2114–2115 were a period of relatively high solar activity and contained several transient events such as flares and CMEs that might have contributed to the model differences at Earth in a complicated way. Therefore, it would be helpful to confirm the results in the previous section by using IPS data from a period of very low solar activity during which interactions between the ambient fast and slow wind streams were the predominant physical processes occurring in interplanetary space. Once again, we examine the solar wind models using boundary values fit to Wind and IPS data for CRs 2058–2063 in 2007, during which

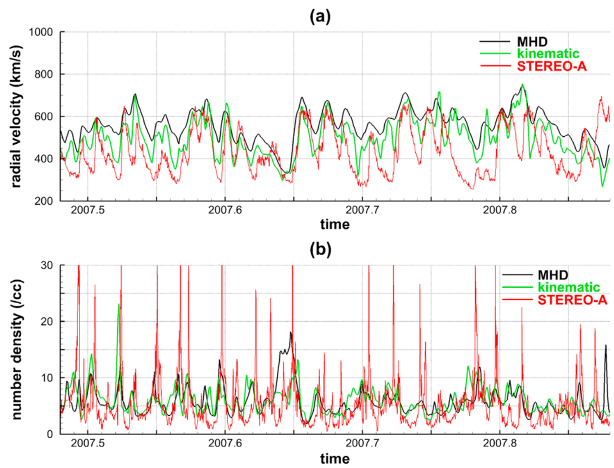

Figure 6. (a) Radial velocity (km s^{-1}) and (b) proton number density (cm^{-3}) at STEREO-A for CRs 2058–2063 (21 June to 1 December 2007). One hour averages of in situ measurements are shown as reference. The MHD solution is shown in black, while the in situ data and kinematic values are shown in red and green, respectively.

very few ICMEs were identified by the STEREO spacecraft and/or in the near-Earth environment [*Kilpua et al.*, 2009; *Richardson and Cane*, 2010].

In Figures 5–8, we show the radial velocity and number density comparisons at Earth, STEREO-A, STEREO-B, and Ulysses for CRs 2058–2063. Since this was a mostly quiet, uneventful period, it is safe to assume that most of the fluctuations are due to solar rotation and stream interactions. In fact, Wind and ACE detected over 20 SIRs during this period (http://www-ssc.igpp.ucla.edu/~jlan/ACE/Level3/SIR_List_from_Lan_Jian.pdf), which are easily identified by sharp density spikes and steep velocity increases in the OMNI data in Figure 5. Once again, the kinematic reconstruction of the proton radial velocity and number density closely match OMNI data at Earth. Meanwhile, radial velocity is generally much larger (by up to 150 km s^{-1}) in the MHD solution than in the kinematic solution. The density fluctuations are also much larger in the MHD model than in the kinematic model, which confirms what we have seen earlier.

As shown in Figures 6 and 7, the MHD solution exhibits the same pattern at STEREO-A and STEREO-B as at Earth, i.e., larger density fluctuations and radial velocity compared to the kinematic solution. More interestingly, the kinematic velocity and density match STEREO measurements much better this time than in 2011. However, we point out that the kinematic radial velocity is generally greater (by up to 200 km s^{-1}) than in situ data. The discrepancy is particularly large at STEREO-A for the latter half of the period. As for proton density, the kinematic solution shows smaller fluctuations compared to in situ data for most of the period at both spacecraft. Overall, the kinematic solution appears to be in better agreement with spacecraft data at STEREO-B than at STEREO-A, which is most likely due to the smaller longitudinal offset between STEREO-B and Earth because STEREO-A and STEREO-B were 15° and 10° ahead and behind Earth at the time, respectively. This shows that while the kinematic reconstruction remains fairly accurate within 20° of Earth, the accuracy may fall rapidly as the longitudinal distance from Earth increases as we see in Figure 4. However, we must note that the large discrepancies in the kinematic solution at STEREO, in 2011, for example, may in part be due to a lack of sufficient number of IPS lines of sight in those directions during some portions of that period.

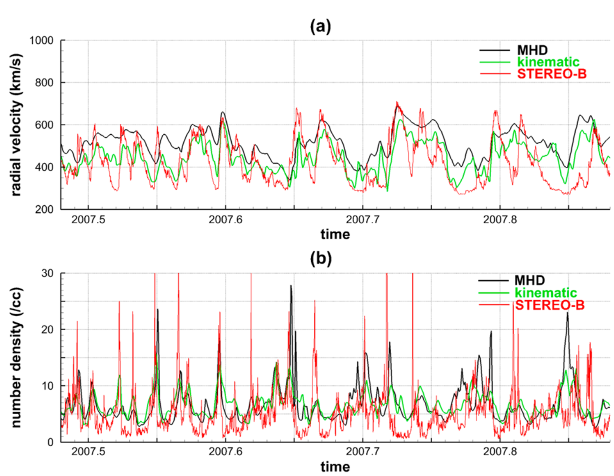

Figure 7. (a) Radial velocity (km s^{-1}) and (b) proton number density (cm^{-3}) at STEREO-B for CRs 2058–2063 (21 June to 1 December 2007). One hour averages of in situ measurements are shown as reference. The MHD solution is shown in black, while the in situ data and kinematic values are shown in red and green, respectively.

Figure 8 shows the radial velocity and number density comparisons at Ulysses. Again, we generally observe the same large differences in radial velocity between the MHD and kinematic models as seen at Earth. We should note that Ulysses moved from the heliographic latitude of −40° to +70° while passing the perihelion at 1.39 AU in the middle

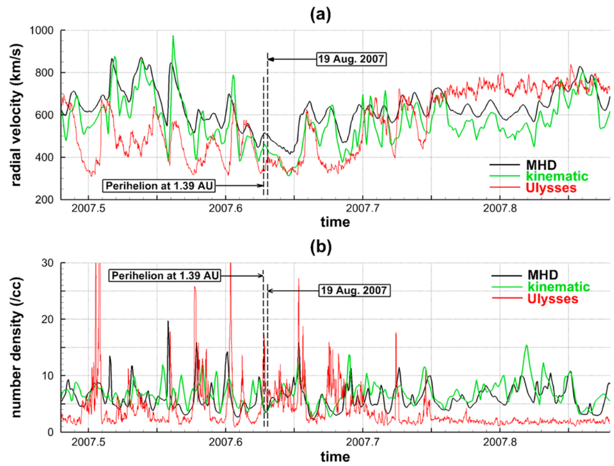

Figure 8. (a) Radial velocity (km s^{-1}) and (b) proton number density (cm^{-3}) at Ulysses for CRs 2058–2063 (21 June to 1 December 2007). One hour averages of in situ measurements are shown as reference. The MHD solution is shown in black, while the in situ data and kinematic values are shown in red and green, respectively. Number density is scaled to 1 AU assuming a R^{-2} dependence.

of the period. As Ulysses crossed the ecliptic plane on 19 August 2007, it came within 12° of Earth longitudinally. The fluctuations in radial velocity show a relatively good overlap between the kinematic solution and the Ulysses measurements in the middle of the period when Ulysses is near the perihelion and around the ecliptic plane. However, at other times when Ulysses is at middle to high latitudes and somewhat farther out, the radial velocity in the kinematic solution is dramatically overestimated at the southern heliographic latitudes and consistently underestimated at the northern heliographic latitudes compared to in situ measurements. Furthermore, the proton number density in the kinematic model appears to be not as accurately reproduced as at Earth, especially at the northern heliographic latitudes where it shows large fluctuations both in density and velocity that were not observed by Ulysses. Again, some of the large discrepancies of the kinematic solution at high heliographic latitudes may be attributed to insufficient number of IPS lines of sight.

5. Fitting the MHD Model to In Situ Measurements

5.1. CRs 2114–2115 (26 August to 19 October 2011): Boundary Velocity Reduced by 10%

The MHD and kinematic solar wind models produce substantially different results at Earth in part due to the lack of acceleration in the kinematic model. Therefore, it is likely that the radial velocities at the 0.25 AU boundary are somewhat overestimated in the kinematic model, and this produces generally larger velocities at 1 AU in a MHD model. While it would be best to restrict any modification of the boundary values to take place within the tomography program, it is interesting to see how a MHD solution would change with a slightly modified boundary data set. Thus, we make a simple adjustment to the kinematic boundary data for CRs 2114–2115 by reducing the radial velocity by 10%. The results are shown in Figures 9a and 9b along with OMNI 1 h averaged data and the kinematic solution. Though the discrepancy between the models remains somewhat large at around 2011.8, the MHD radial velocity shows much better agreement with the OMNI and the kinematic values throughout the period. Since the proton velocity is smaller by 10% at the inner boundary now, solar wind structures of different speeds have longer time to interact with each other between 0.25 and 1 AU in the MHD model and thus produce slightly larger density fluctuations at Earth.

Although in situ measurements of the solar wind velocity or density are not available for comparison at Mercury and Venus during this time period, it is still interesting to see how the reduced boundary velocity changes the MHD solution at these locations. Since the observations of IPS allow for the determination of the solar wind velocity at distances around 0.25 AU to 0.75 AU rather than precisely at the Earth, we assume that the kinematic velocities, which have been adjusted to closely match IPS data, can serve as reference values in this region. Therefore, we extract the MHD solutions at Mercury and Venus and present them in Figures 9c–9f. The MHD results from the reduced boundary velocity are shown in blue while the original MHD results and the kinematic solution are shown in black and green, respectively.

During CRs 2114–2115, the heliocentric distance of Mercury varies between 0.3 and 0.45 AU. Thus, the MHD (black line) and the kinematic radial velocities are nearly identical in the first third of the period as shown in Figure 9c when Mercury remains mostly at 0.3 AU, which is just above the inner boundary. However, as Mercury moves out from 0.3 to 0.45 AU in the second third of the period, the radial velocity difference steadily grows until it reaches about 50 km s^{-1}. The density comparison in Figure 9d shows nearly identical

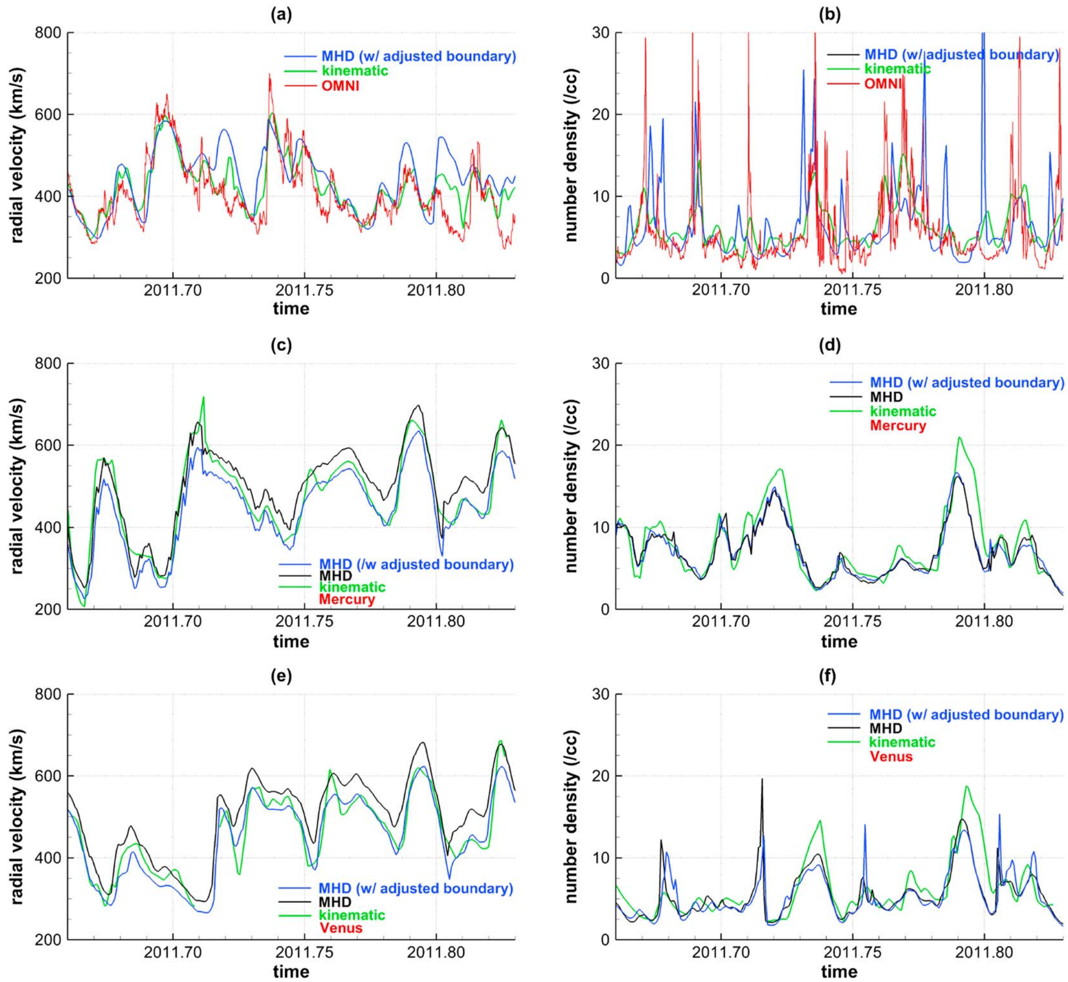

Figure 9. Radial velocity (km s^{-1}) and proton number density (cm^{-3}) at (a and b) Earth, (c and d) Mercury, and (e and f) Venus for CRs 2114–2115 (26 August to 19 October 2011). Number density is scaled to 1 AU assuming a R^{-2} dependence. The MHD solutions obtained with boundary radial velocities reduced by 10% are shown in blue, whereas the kinematic solutions are represented by green. At Earth, we show OMNI 1 h averages in red. At Mercury and Venus, we also show the MHD solutions from unmodified boundary values in black.

values initially, but as radial velocity grows with increasing heliocentric distance, the MHD solution deviates to somewhat smaller values than the kinematic density. This is expected since the solar wind is expanding faster at 0.45 AU in the MHD model than in the kinematic model.

With the radial velocity at the inner boundary reduced by 10%, the MHD results (blue line) at Mercury are as much as 50 km s^{-1} lower than the kinematic values in the first third of the period (at around 0.3 AU), but they match the kinematic solution better at 0.45 AU now. It appears that the reduction of the boundary velocity has caused no significant changes in the MHD density at Mercury as shown in Figure 9d.

We also look at Venus whose heliocentric distance stays almost constant at 0.72 AU during the period. While there are a few places where the discrepancy in the MHD solution (black line) is unusually large, such as at 2011.72 where the difference is greater than 100 km s^{-1} in Figure 9e, the amount of the velocity difference is around 50 km s^{-1}, similar to what we see at Mercury. More interestingly, with the reduced boundary velocity, the MHD solution (blue line) agrees better with the kinematic velocity at Venus. However, as shown in Figure 9f, the modification of the boundary velocity has caused relatively larger changes in density than at Mercury. For example, the density peaks are significantly smaller at 2011.71–2011.72 or larger at 2011.75–2011.76 and 2011.805–2011.820. In general, the difference between the MHD and the kinematic densities grows somewhat larger with smaller boundary velocities.

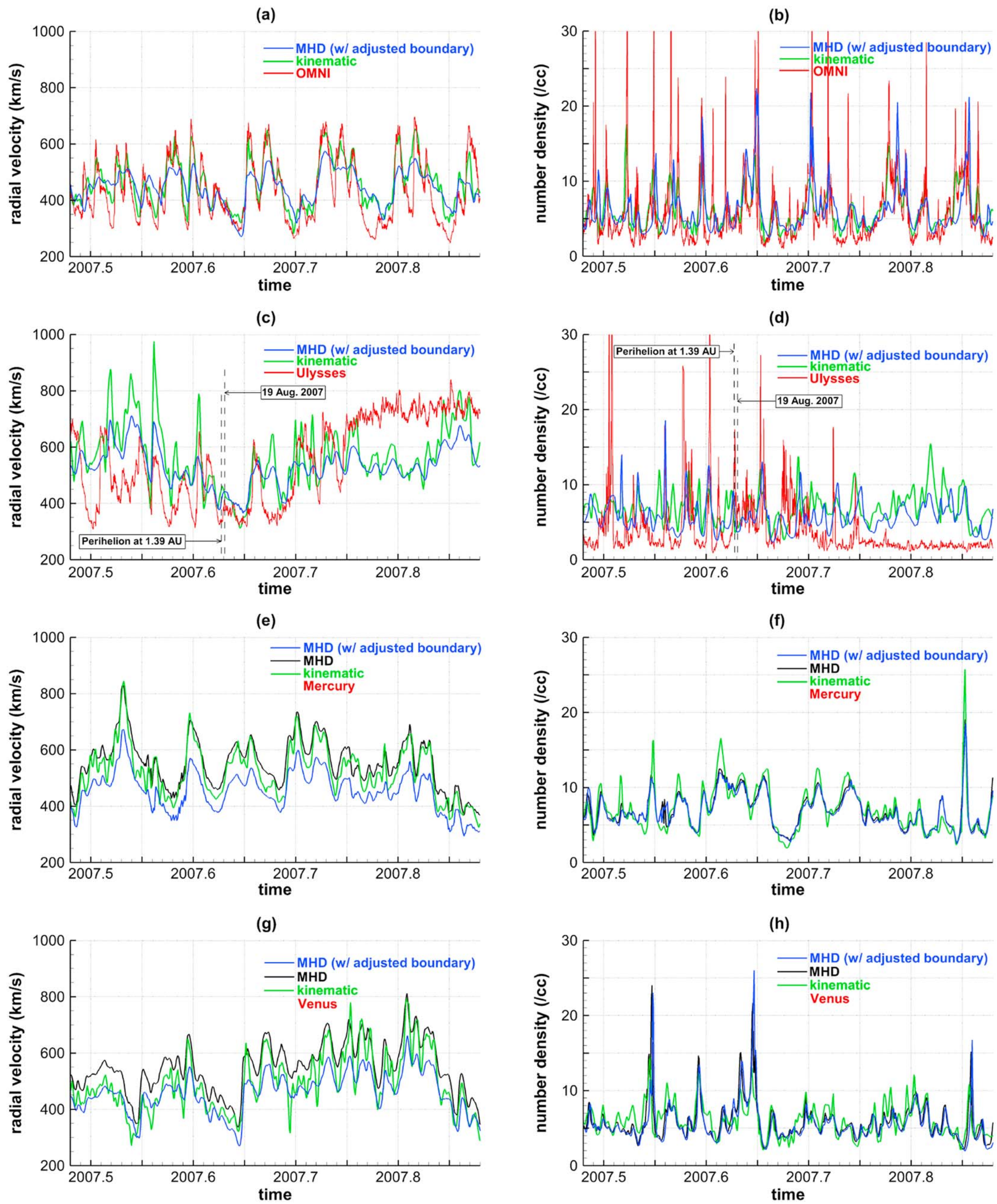

Figure 10. Radial velocity (km s^{-1}) and proton number density (cm^{-3}) at (a and b) Earth, (c and d) Ulysses, (e and f) Mercury, and (g and h) Venus for CRs 2058–2063 (21 June to 1 December 2007). Number density is scaled to 1 AU assuming a R^{-2} dependence. The MHD solutions obtained with boundary radial velocities reduced by 20% are shown in blue, whereas the kinematic solutions are represented by green. At Earth and Ulysses, we show 1 h averages of in situ data in red. At Mercury and Venus, we also show the MHD solutions from unmodified boundary values in black.

5.2. CRs 2058–2063 (21 June to 1 December 2007): Boundary Velocity Reduced by 20%

For CRs 2058–2063, we reduce the boundary velocity by 20% to achieve the best match at Earth. The MHD results at Earth are shown together with OMNI data and the kinematic solution in Figures 10a and 10b, while we also provide comparisons at Ulysses in Figures 10c and 10d. Comparisons of the MHD models (with or without the 20% change in the boundary velocities) to the kinematic solution at Mercury and Venus are shown in Figures 10e and 10h.

At Earth and Ulysses, the MHD velocity (blue line) matches the kinematic solution better while there are no significant changes in density. As a result, the smaller MHD velocity at Ulysses shows somewhat better agreement with in situ data around the ecliptic plane in the middle of the period, but there are still large discrepancies at higher latitudes. In the last third of the period when the spacecraft travels from the heliographic latitude of +30° to +70°, the MHD velocity is 200 km s^{-1} lower than the in situ measurements. To improve the MHD velocity at high latitudes, it is obvious that more complicated adjustments are needed.

At Mercury, the MHD velocity (blue line) is much smaller (by up to 20%) than the kinematic velocity, while the MHD density shows little change at both Mercury and Venus. The difference between the MHD and the kinematic radial velocities at Venus is generally smaller than at Mercury but still quite large. It appears that a 10% reduction in the boundary velocity would produce better agreement between the MHD and the kinematic velocities at Venus as it did in CRs 2114–2115.

Further tweaking of the boundary values by adjusting the densities or modifying the velocities in more complicated ways might help to fit the MHD results more closely with OMNI and Ulysses data. However, it would be difficult to ensure that the resulting 3-D MHD solution produces reasonable results within 1 AU. It is clear that any ad hoc modifications of the boundary values should be done with an eye to the physical properties governing the outward flow of the solar wind.

6. Summary and Discussions

We have used the UCSD time-dependent tomography results fit to STEL IPS and Wind data for CRs 2114–2115 and 2058–2063 as inner boundary conditions in an MHD heliospheric model. Since the MHD heliospheric model can provide physically accurate description of the 3-D large-scale solar wind structure throughout the inner heliosphere, we anticipate that an MHD model driven by IPS-based time-varying boundary values would reproduce the fluctuations in solar wind parameters at Earth and various spacecraft trajectories with reasonable accuracy. This is a fair expectation because the current version of the time-dependent tomography consistently reproduces the proton radial velocity and number density at Earth with remarkable accuracy. Eventually, we may extrapolate the MHD reconstruction of the inner heliosphere to the region bounding the LISM using a more complicated model, such as the multifluid or the MHD-kinetic model available in MS-FLUKSS, which accounts for the charge exchange process between ions and neutrals and the pickup ion effects that greatly influence the structure of the outer heliosphere.

In an earlier MHD analysis using kinematic inner boundary values fit to STEL IPS and Wind data [*Kim et al.*, 2014], we suspected potentially large errors associated with multiple steps of interpolation at the boundary contributing to the model differences at Earth. By significantly boosting both the spatial and temporal resolution of the boundary data, we have minimized the error due to interpolation that may be a nontrivial factor in the presence of transient structures. Our results imply that fundamental differences between the MHD and kinematic models—i.e., acceleration in the MHD model and the stream interaction dynamics—cause a considerable discrepancy between the MHD solution and in situ measurements at Earth. For the most part, the MHD velocities are markedly higher than both OMNI and the kinematic model values for CRs 2114–2115 and 2058–2063, while the density fluctuations generally grow larger with distance in the MHD model than in the kinematic model. The discrepancy between the kinematic and MHD solutions for the same boundary conditions indicates obvious differences between the two models.

Although it may be possible to enhance the MHD solution in the vicinity of Earth by adjusting the boundary values in an ad hoc fashion, such approach must be taken with great care to ensure that the resulting 3-D MHD solution maintains reasonable agreement with IPS data. This would be difficult to achieve outside the tomography program. Therefore, a more prudent approach would be to fully replace the kinematic solar wind model in the time-dependent tomography with an MHD model as suggested by *Jackson et al.* [2007b] and *Bisi et al.* [2008]. By doing so, the iteratively fit heliospheric MHD model would provide more reliable solar wind reconstruction within the entire computational domain. This upgrade to the time-dependent tomography would be a big first step in mapping the global heliosphere by delivering better, more realistic inputs to outer heliosphere models. Furthermore, it would be immensely helpful in analyzing the plasma measurements by Solar Probe Plus, which will begin exploring the vast region between 1 AU and roughly 10 R_s in the future.

On a side note, it would be interesting to use another source of IPS data that provides much larger number of observations per day, such as the Ootacamund (Ooty) Radio Telescope in India [*Manoharan*, 2009]. The larger number of IPS observations (approximately 1000 sources per day for Ooty) would allow us to use

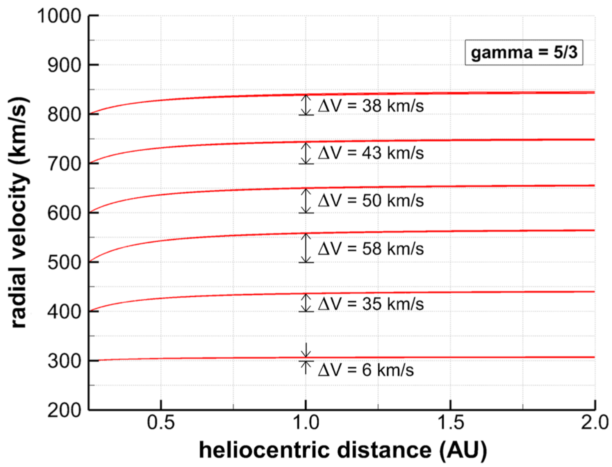

Figure A1. The proton radial velocity (km s^{-1}) of a stationary, isotropic, spherically symmetric solar wind in the MS-FLUKSS MHD model between 0.25 and 2 AU.

higher resolution in the tomography that may improve the solar wind reconstruction, particularly at high heliographic latitudes where fewer number of observations are available. In fact, *Bisi et al.* [2009b] have analyzed tomographic reconstructions from both STEL and Ooty IPS data for early November 2004, which was an active period of geomagnetic activity, and showed that the Ooty reconstructions for that period were better than the STEL IPS and/or SMEI reconstructions. Therefore, it may be worthwhile to repeat the MHD analysis using time-dependent tomography results fit to Ooty data to confirm the findings in this study. However, it is clear that the UCSD tomography results used in this paper provide the best fit to observational data only in the framework of the kinematic solar wind model. At each iterative step the kinematic tomographic forward modeling simulation provides a more accurate 3-D representation of the solar wind by converging to a better inner boundary. The observed difference in the results obtained in these iterative steps is directly related to the discrepancies in the MHD and kinematic descriptions of the solar wind. Only a time-dependent MHD tomography would make it possible both to fit solar wind data (IPS and in situ, as done in a kinematic IPS tomography) and derive the inner boundary conditions more consistent with our MHD model.

Appendix A: Radial Velocity Test

In Figure A1, we show how the proton radial velocity changes from 0.25 to 2 AU in an adiabatically expanding, isotropic, spherically symmetric MHD solar wind model. For a stream with a particular radial velocity (e.g., 300, 400, 500, 600, 700, and 800 km s^{-1}) and magnetic field at 0.25 AU, we assign proton number density and temperature using correlation functions $N(V)$ and $T(V)$ determined from in situ measurements of the ambient solar wind by the Ulysses spacecraft [*Ebert et al.*, 2009; *Pogorelov et al.*, 2013b]. In this extremely simple test case, we see minimal to moderate increases in radial velocity (up to approximately 60 km s^{-1}) from 0.25 to 1 AU. The acceleration is almost negligible beyond 1 AU.

Acknowledgments
This research was supported by NASA grants NNX09AW44G, NNX10AE46G, NNX09AP74A, and NNX12AB30G and also by NSF PRAC grant OCI-1053575. The computations were performed on Kraken Cray XT5 at the National Institute for Computational Sciences and on SGI Pleiades at the NASA Advanced Supercomputing Division. The authors are grateful to the two anonymous reviewers who thoroughly assessed this work and provided many critical comments. Furthermore, T.K. Kim acknowledges support by the Alabama EPSCoR Graduate Research Scholars Program and the NSF EAPSI fellowship.

Yuming Wang thanks Mario Bisi and another reviewer for their assistance in evaluating this paper.

References

Armstrong, J. W., and W. A. Coles (1972), Analysis of three-station interplanetary scintillation, *J. Geophys. Res.*, *77*, 4602–4610, doi:10.1029/JA077i025p04602.

Asai, K., M. Kojima, M. Tokumaru, A. Yokobe, B. V. Jackson, P. L. Hick, and P. K. Manoharan (1998), Heliospheric tomography using interplanetary scintillation observations. III—Correlation between speed and electron density fluctuations in the solar wind, *J. Geophys. Res.*, *103*, 1991–2001, doi:10.1029/97JA02750.

Bame, S. J., D. J. McComas, B. L. Barraclough, J. L. Phillips, K. J. Sofaly, J. C. Chavez, B. E. Goldstein, and R. K. Sakurai (1992), The Ulysses solar wind plasma experiment, *Astron. Astrophys. Suppl. Ser.*, *92*, 237–265.

Bisi, M. M., R. A. Fallows, A. R. Breen, S. Rifai Habbal, and R. A. Jones (2007), Large-scale structure of the fast solar wind, *J. Geophys. Res.*, *112*, A06101, doi:10.1029/2006JA012166.

Bisi, M. M., B. V. Jackson, P. P. Hick, A. Buffington, D. Odstrcil, and J. M. Clover (2008), Three-dimensional reconstructions of the early November 2004 coordinated data analysis workshop geomagnetic storms: Analyses of STELab IPS speed and SMEI density data, *J. Geophys. Res.*, *113*, A00A11, doi:10.1029/2008JA013222.

Bisi, M. M., B. V. Jackson, A. Buffington, J. M. Clover, P. P. Hick, and M. Tokumaru (2009a), Low-resolution STELab IPS 3D reconstructions of the whole heliosphere interval and comparison with in-ecliptic solar wind measurements from STEREO and Wind instrumentation, *Sol. Phys.*, *256*, 201–217, doi:10.1007/s11207-009-9350-9.

Bisi, M. M., B. V. Jackson, J. M. Clover, P. K. Manoharan, M. Tokumaru, P. P. Hick, and A. Buffington (2009b), 3-D reconstructions of the early-November 2004 CDAW geomagnetic storms: Analysis of Ooty IPS speed and density data, *Ann. Geophys.*, *27*, 4479–4489, doi:10.5194/angeo-27-4479-2009.

Bisi, M. M., R. A. Fallows, A. R. Breen, and I. J. O'Neill (2010a), Interplanetary scintillation observations of stream interaction regions in the solar wind, *Sol. Phys.*, *261*, 149–172, doi:10.1007/s11207-009-9471-1.

Bisi, M. M., et al. (2010b), From the Sun to the Earth: The 13 May 2005 coronal mass ejection, *Sol. Phys.*, *265*, 49–127, doi:10.1007/s11207-010-9602-8.

Bisi, M. M., B. V. Jackson, P. P. Hick, A. Buffington, J. M. Clover, M. Tokumaru, and K. Fujiki (2010c), Three-dimensional reconstructions and mass determination of the 2008 June 2 LASCO coronal mass ejection using STELab interplanetary scintillation observations, *Astrophys. J. Lett.*, *715*, L104–L108, doi:10.1088/2041-8205/715/2/L104.

Borovikov, S. N., I. A. Kryukov, and N. V. Pogorelov (2009), Adaptive mesh refinement on curvilinear grids, in *Numerical Modeling of Space Plasma Flows: ASTRONUM-2008, Astronomical Society of the Pacific Conference Series*, vol. 406, edited by N. V. Pogorelov et al., p. 127, ASP, San Francisco, Calif.

Borovikov, S. N., J. Heerikhuisen, and N. V. Pogorelov (2013), Hybrid parallelization of adaptive MHD-kinetic module in multi-scale fluid-kinetic simulation suite, in *Numerical Modeling of Space Plasma Flows (ASTRONUM2012)*, vol. 474, edited by N. V. Pogorelov, E. Audit, and G. P. Zank, p. 219, Astron. Soc. of the Pacific Conf. Ser., San Francisco, Calif.

Bourgois, G., G. Daigne, W. A. Coles, J. Silen, T. Turunen, and P. J. Williams (1985), Measurements of the solar wind velocity with EISCAT, *Astron. Astrophys.*, *144*, 452–462.

Breen, A. R., P. J. Moran, C. A. Varley, P. J. S. Williams, W. A. Coles, R. R. Grall, M. T. Klinglesmith, and J. Markkanen (1997), EISCAT measurements of interaction regions in the solar wind, *Adv. Space Res.*, *20*, 27–30, doi:10.1016/S0273-1177(97)00475-4.

Breen, A. R., P. J. Moran, C. A. Varley, W. P. Wilkinson, P. J. S. Williams, W. A. Coles, A. Lecinski, and J. Markkanen (1998), Interplanetary scintillation observations of interaction regions in the solar wind, *Ann. Geophys.*, *16*, 1265–1282, doi:10.1007/s00585-998-1265-5.

Breen, A. R., P. Riley, A. J. Lazarus, A. Canals, R. A. Fallows, J. Linker, and Z. Mikic (2002), The solar wind at solar maximum: Comparisons of EISCAT IPS and in situ observations, *Ann. Geophys.*, *20*, 1291–1309, doi:10.5194/angeo-20-1291-2002.

Breen, A. R., R. A. Fallows, M. M. Bisi, P. Thomasson, C. A. Jordan, G. Wannberg, and R. A. Jones (2006), Extremely long baseline interplanetary scintillation measurements of solar wind velocity, *J. Geophys. Res.*, *111*, A08104, doi:10.1029/2005JA011485.

Briggs, B. H., G. J. Phillips, and D. H. Shinn (1950), The analysis of observations on spaced receivers of the fading of radio signals, *Proc. Phys. Soc. B*, *63*, 106–121, doi:10.1088/0370-1301/63/2/305.

Coles, W. A. (1978), Interplanetary scintillation, *Space Sci. Rev.*, *21*, 411–425, doi:10.1007/BF00173067.

Coles, W. A. (1995), Interplanetary scintillation observations of the high-latitude solar wind, *Space Sci. Rev.*, *72*, 211–222, doi:10.1007/BF00768782.

Coles, W. A. (1996), A bimodal model of the solar wind speed, *Astrophys. Space Sci.*, *243*, 87–96, doi:10.1007/BF00644037.

Coles, W. A., and J. J. Kaufman (1978), Solar wind velocity estimation from multi-station IPS, *Radio Sci.*, *13*, 591–597, doi:10.1029/RS013i003p00591.

Coles, W. A., J. K. Harmon, A. J. Lazarus, and J. D. Sullivan (1978), Comparison of 74-MHz interplanetary scintillation and IMP 7 observations of the solar wind during 1973, *J. Geophys. Res.*, *83*, 3337–3341, doi:10.1029/JA083iA07p03337.

Dennison, P. A., and A. Hewish (1967), The solar wind outside the plane of the ecliptic, *Nature*, *213*, 343–346, doi:10.1038/213343a0.

Dunn, T., B. V. Jackson, P. P. Hick, A. Buffington, and X. P. Zhao (2005), Comparative analyses of the CSSS calculation in the UCSD tomographic solar observations, *Sol. Phys.*, *227*, 339–353, doi:10.1007/s11207-005-2759-x.

Ebert, R. W., D. J. McComas, H. A. Elliott, R. J. Forsyth, and J. T. Gosling (2009), Bulk properties of the slow and fast solar wind and interplanetary coronal mass ejections measured by Ulysses: Three polar orbits of observations, *J. Geophys. Res.*, *114*, A01109, doi:10.1029/2008JA013631.

Eyles, C. J., G. M. Simnett, M. P. Cooke, B. V. Jackson, A. Buffington, P. P. Hick, N. R. Waltham, J. M. King, P. A. Anderson, and P. E. Holladay (2003), The Solar Mass Ejection Imager (SMEI), *Sol. Phys.*, *217*, 319–347, doi:10.1023/B:SOLA.0000006903.75671.49.

Fallows, R. A., P. J. S. Williams, and A. R. Breen (2002), EISCAT measurements of solar wind velocity and the associated level of interplanetary scintillation, *Ann. Geophys.*, *20*, 1279–1289, doi:10.5194/angeo-20-1279-2002.

Fallows, R. A., A. R. Breen, M. M. Bisi, R. A. Jones, and G. Wannberg (2006), Dual-frequency interplanetary scintillation observations of the solar wind, *Geophys. Res. Lett.*, *33*, L11106, doi:10.1029/2006GL025804.

Fallows, R. A., A. R. Breen, and G. D. Dorrian (2008), Developments in the use of EISCAT for interplanetary scintillation, *Ann. Geophys.*, *26*, 2229–2236, doi:10.5194/angeo-26-2229-2008.

Galvin, A. B., et al. (2008), The Plasma and Suprathermal Ion Composition (PLASTIC) investigation on the STEREO observatories, *Space Sci. Rev.*, *136*, 437–486, doi:10.1007/s11214-007-9296-x.

Gapper, G. R., A. Hewish, A. Purvis, and P. J. Duffett-Smith (1982), Observing interplanetary disturbances from the ground, *Nature*, *296*, 633–636, doi:10.1038/296633a0.

Goelzer, M. L., N. A. Schwadron, and C. W. Smith (2014), An analysis of Alfvén radius based on sunspot number from 1749 to today, *J. Geophys. Res. Space Physics*, *119*, 115–120, doi:10.1002/2013JA019420.

Grall, R. R. (1995), Remote sensing observations of the solar wind near the Sun, PhD thesis, Univ. of California, San Diego, Calif.

Hayashi, K. (2012), An MHD simulation model of time-dependent co-rotating solar wind, *J. Geophys. Res.*, *117*, A08105, doi:10.1029/2011JA017490.

Hayashi, K., M. Kojima, M. Tokumaru, and K. Fujiki (2003), MHD tomography using interplanetary scintillation measurement, *J. Geophys. Res.*, *108*, 1102, doi:10.1029/2002JA009567.

Hayashi, K., M. Tokumaru, K. Fujiki, and M. Kojima (2011), Three-dimensional solar wind structures obtained with MHD simulation model using observation-based time-varying inner boundary map, in *5th International Conference of Numerical Modeling of Space Plasma Flows (ASTRONUM 2010)*, vol. 444, edited by N. V. Pogorelov, E. Audit, and G. P. Zank, p. 111, Astron. Soc. of the Pacific Conf. Ser., San Francisco, Calif.

Hayashi, K., H. Washimi, and M. Tokumaru (2012), The MHD simulation of the inner heliosphere over 9 years using the observation-based time-varying boundary data, in *Proceedings of 10th Annual International Astrophysics Conference,* vol. 1436, J. Heerikhuisen et al., pp. 308–313, Am. Inst. of Phys. Conf. Ser., Melville, N. Y., doi:10.1063/1.4723624.

Hewish, A., and S. Bravo (1986), The sources of large-scale heliospheric disturbances, *Sol. Phys.*, *106*, 185–200, doi:10.1007/BF00161362.

Hewish, A., P. F. Scott, and D. Wills (1964), Interplanetary scintillation of small diameter radio sources, *Nature*, *203*, 1214–1217, doi:10.1038/2031214a0.

Jackson, B. V., and P. P. Hick (2004), Three-dimensional tomography of interplanetary disturbances, in *Solar and Space Weather Radio-physics,* vol. 314, edited by D. E. Gary and C. U. Keller, pp. 355–386, Astrophys. Space Sci. Library, Springer, Houten, Netherlands, doi:10.1007/1-4020-2814-8_17.

Jackson, B. V., P. L. Hick, M. Kojima, and A. Yokobe (1998), Heliospheric tomography using interplanetary scintillation observations 1. Combined Nagoya and Cambridge data, *J. Geophys. Res.*, *103*, 12,049–12,068, doi:10.1029/97JA02528.

Jackson, B. V., P. P. Hick, A. Buffington, M. Kojima, M. Tokumaru, K. Fujiki, T. Ohmi, and M. Yamashita (2003), Time-dependent tomography of hemispheric features using interplanetary scintillation (IPS) remote-sensing observations, in *Solar Wind Ten: Proceedings of the Tenth International Solar Wind Conference,* vol. 679, edited by M. Velli et al., pp. 75–78, Am. Inst. of Phys. Conf. Ser., Melville, N. Y., doi:10.1063/1.1618545.

Jackson, B. V., et al. (2004), The Solar Mass Ejection Imager (SMEI) mission, *Sol. Phys.*, *225*, 177–207, doi:10.1007/s11207-004-2766-3.

Jackson, B. V., A. Buffington, P. P. Hick, X. Wang, and D. Webb (2006), Preliminary three-dimensional analysis of the heliospheric response to the 28 October 2003 CME using SMEI white-light observations, *J. Geophys. Res.*, *111*, A04S91, doi:10.1029/2004JA010942.

Jackson, B. V., P. P. Hick, A. Buffington, M. M. Bisi, M. Kojima, and M. Tokumaru (2007a), Comparison of the extent and mass of CME events in the interplanetary medium using IPS and SMEI Thomson scattering observations, *Astron. Astrophys. Trans.*, *26*, 477–487, doi:10.1080/10556790701612221.

Jackson, B. V., J. A. Boyer, P. P. Hick, A. Buffington, M. M. Bisi, and D. H. Crider (2007b), Analysis of solar wind events using interplanetary scintillation remote sensing 3D reconstructions and their comparison at Mars, *Sol. Phys.*, *241*, 385–396, doi:10.1007/s11207-007-0276-9.

Jackson, B. V., P. P. Hick, M. M. Bisi, J. M. Clover, and A. Buffington (2010), Inclusion of in-situ velocity measurements into the UCSD time-dependent tomography to constrain and better-forecast remote-sensing observations, *Sol. Phys.*, *265*, 245–256, doi:10.1007/s11207-010-9529-0.

Jackson, B. V., P. P. Hick, A. Buffington, M. M. Bisi, J. M. Clover, M. Tokumaru, M. Kojima, and K. Fujiki (2011), Three-dimensional reconstruction of heliospheric structure using iterative tomography: A review, *J. Atmos. Sol. Terr. Phys.*, *73*, 1214–1227, doi:10.1016/j.jastp.2010.10.007.

Jackson, B. V., J. M. Clover, P. P. Hick, A. Buffington, M. M. Bisi, and M. Tokumaru (2013), Inclusion of real-time in-situ measurements into the UCSD time-dependent tomography and its use as a forecast algorithm, *Sol. Phys.*, *285*, 151–165, doi:10.1007/s11207-012-0102-x.

Jian, L. K., C. T. Russell, J. G. Luhmann, A. B. Galvin, and K. D. C. Simunac (2013), Solar wind observations at STEREO: 2007–2011, in *SOLAR WIND 13: Proceedings of the Thirteenth International Solar Wind Conference, Am. Inst. of Phys. Conf. Ser.,* vol. 1539, edited by G. P. Zank et al., pp. 191–194, AIP Conf. Proc., Melville, N. Y., doi:10.1063/1.4811020.

Kakinuma, T., and M. Kojima (1984), Three-station observations of interplanetary scintillation at 327 MHz. I, *Proc. Res. Inst. Atmos. Nagoya Univ.*, *31*, 1–10.

Kakinuma, T., H. Washimi, and M. Kojima (1973), On the analysis of the observations of interplanetary scintillations obtained with three spaced receivers, *Publ. Astron. Soc. Jpn.*, *25*, 271.

Kilpua, E. K. J., J. Pomoell, A. Vourlidas, R. Vainio, J. Luhmann, Y. Li, P. Schroeder, A. B. Galvin, and K. Simunac (2009), STEREO observations of interplanetary coronal mass ejections and prominence deflection during solar minimum period, *Ann. Geophys.*, *27*, 4491–4503, doi:10.5194/angeo-27-4491-2009.

Kim, T. K., N. V. Pogorelov, S. N. Borovikov, and K. Hayashi (2012), Numerical modeling of solar wind flow using interplanetary scintillation data as boundary conditions, in *Numerical Modeling of Space Plasma Slows (ASTRONUM 2011), Astron. Soc. of the Pacific Conf. Ser.*, vol. 459, edited by N. V. Pogorelov et al., p. 209, ASP, San Francisco, Calif.

Kim, T. K., N. V. Pogorelov, S. N. Borovikov, K. Hayashi, B. V. Jackson, M. Tokumaru, and H.-S. Yu (2014), Modeling the global heliosphere using IPS-derived time-dependent boundary conditions, in *Outstanding Problems in Heliophysics: From Coronal Heating to the Edge of the Heliosphere, Astron. Soc. of the Pacific Conf. Ser.*, vol. 484, edited by Q. Hu and G. P. Zank, pp. 92–98, ASP, San Francisco, Calif.

Klinglesmith, M. (1997), The polar solar wind from 2.5 to 40 solar radii: Results of intensity scintillation measurements, PhD thesis, Univ. of California, San Diego, Calif.

Kojima, M. (1979), Anisotropic structure of solar-wind plasma irregularities observed with interplanetary scintillations, *Publ. Astron. Soc. Jpn.*, *31*, 231–250.

Kojima, M., and T. Kakinuma (1986), Three-station observations of interplanetary scintillation at 327 MHz. II—Evolution of two-dimensional solar wind speed structure during 1983 to 1985, *Nagoya Univ. Res. Inst. Atmos. Proc.*, *33*, 1–18.

Kojima, M., and T. Kakinuma (1990), Solar cycle dependence of global distribution of solar wind speed, *Space Sci. Rev.*, *53*, 173–222, doi:10.1007/BF00212754.

Kojima, M., Y. Ishida, K. Maruyama, and T. Kakinuma (1982), An observation system of interplanetary scintillation at UHF, *Nagoya Univ. Res. Inst. Atmos. Proc.*, *29*, 61–83.

Kojima, M., M. Tokumaru, H. Watanabe, A. Yokobe, K. Asai, B. V. Jackson, and P. L. Hick (1998), Heliospheric tomography using interplanetary scintillation observations: 2. Latitude and heliocentric distance dependence of solar wind structure at 0.1–1 AU, *J. Geophys. Res.*, *103*, 1981–1990, doi:10.1029/97JA02162.

Kojima, M., W. A. Coles, M. Tokumaru, and K. Fujiki (2013), Scintillation measurements of the solar wind velocity in strong scattering near the Sun, *Sol. Phys.*, *283*, 519–540, doi:10.1007/s11207-012-0207-2.

Kryukov, I. A., S. N. Borovikov, N. V. Pogorelov, and G. P. Zank (2006a), Magnetohydrodynamics with Chombo: Tests and first results, in *Numerical Modeling of Space Plasma Flows, Astron. Soc. of the Pacific Conf. Ser.*, vol. 359, edited by G. P. Zank and N. V. Pogorelov, p. 25, ASP, San Francisco, Calif.

Kryukov, I. A., S. N. Borovikov, N. V. Pogorelov, and G. P. Zank (2006b), Multifluid adaptive-mesh simulation of the solar wind interaction with the local interstellar medium, in *Physics of the Inner Heliosheath, Am. Inst. of Phys. Conf. Ser.,* vol. 858, edited by J. Heerikhuisen et al., 39–44, AIP, Melville, N. Y., doi:10.1063/1.2359303.

Kryukov, I. A., S. N. Borovikov, N. V. Pogorelov, and G. P. Zank (2008), A new, three-dimensional, adaptive mesh refinement code for modeling flows of partially ionized plasma, in *Numerical Modeling of Space Plasma Flows, Astron. Soc. of the Pacific Conf. Ser.*, vol. 385, edited by N. V. Pogorelov, E. Audit, and G. P. Zank, p. 265, ASP, San Francisco, Calif.

Kryukov, I. A., N. V. Pogorelov, G. P. Zank, and S. N. Borovikov (2012), Numerical modeling of the solar wind turbulence, in *American Institute of Physics Conference Series, Am. Inst. of Phys. Conf. Ser.,* vol. 1436, edited by J. Heerikhuisen et al., pp. 48–54, AIP, Melville, N. Y., doi:10.1063/1.4723589.

Manoharan, P. K. (2009), Radio scintillation imaging of solar wind structures, in *The Low-Frequency Radio Universe, Astron. Soc. of the Pacific Conf. Ser.*, vol. 407, edited by D. J. Saikia et al., p. 359, ASP, San Francisco, Calif.

Manoharan, P. K. (2012), Three-dimensional evolution of solar wind during solar cycles 22–24, *Astrophys. J.*, *751*, 128, doi:10.1088/0004-637X/751/2/128.

Manoharan, P. K., and S. Ananthakrishnan (1990), Determination of solar-wind velocities using single-station measurements of interplanetary scintillation, *Mon. Not. R. Astron. Soc.*, *244*, 691–695.

Moran, P. J., S. Ananthakrishnan, V. Balasubramanian, A. R. Breen, A. Canals, R. A. Fallows, P. Janardhan, M. Tokumaru, and P. J. S. Williams (2000), Observations of interplanetary scintillation during the 1998 Whole Sun Month: A comparison between EISCAT, ORT and Nagoya data, *Ann. Geophys.*, *18*, 1003–1008, doi:10.1007/s00585-000-1003-0.

Ogilvie, K. W., et al. (1995), SWE, a comprehensive plasma instrument for the wind spacecraft, *Space Sci. Rev.*, *71*, 55–77, doi:10.1007/BF00751326.

Parker, E. N. (1958), Dynamics of the interplanetary gas and magnetic fields, *Astrophys. J.*, *128*, 664, doi:10.1086/146579.

Pogorelov, N. V., G. P. Zank, S. N. Borovikov, V. Florinski, J. Heerikhuisen, and I. A. Kryukov (2008), MHD-neutral model of the outer heliosphere, in *Numerical Modeling of Space Plasma Flows, Astron. Soc. of the Pacific Conf. Ser.*, vol. 385, edited by N. V. Pogorelov, E. Audit, and G. P. Zank, p. 180, ASP, San Francisco, Calif.

Pogorelov, N. V., S. N. Borovikov, V. Florinski, J. Heerikhuisen, I. A. Kryukov, and G. P. Zank (2009), Multi-scale fluid-kinetic simulation suite: A tool for efficient modeling of space plasma flows, in *Numerical Modeling of Space Plasma Flows: ASTRONUM-2008, Astron. Soc. of the Pacific Conf. Ser.*, vol. 406, edited by N. V. Pogorelov et al., p. 149, ASP, San Francisco, Calif.

Pogorelov, N. V., S. N. Borovikov, J. Heerikhuisen, I. A. Kryukov, and G. P. Zank (2010), Modeling heliospheric phenomena with the multi-scale fluid-kinetic simulation suite, in *Numerical Modeling of Space Plasma Flows, Astronum-2009, Astron. Soc. of the Pacific Conf. Ser.*, vol. 429, edited by N. V. Pogorelov, E. Audit, and G. P. Zank, p. 266, ASP, San Francisco, Calif.

Pogorelov, N. V., S. N. Borovikov, J. Heerikhuisen, T. Kim, I. A. Kryukov, and G. P. Zank (2011), Heliospheric modeling with MS-FLUKSS: Interpretation of the IBEX measurements and time-dependent simulations, in *5th International Conference of Numerical Modeling of Space Plasma Flows (ASTRONUM 2010), Astron. Soc. of the Pacific Conf. Ser.*, vol. 444, edited by N. V. Pogorelov, E. Audit, and G. P. Zank, p. 130, ASP, San Francisco, Calif.

Pogorelov, N. V., S. N. Borovikov, L. F. Burlaga, R. W. Ebert, J. Heerikhuisen, Q. Hu, I. A. Kryukov, S. T. Suess, and G. P. Zank (2012a), Numerical modeling of transient phenomena in the distant solar wind and in the heliosheath, in *Physics of the Heliosphere: A 10 Year Retrospective, Proc. 10th Annual Astrophysics Conference, Am. Inst. of Phys. Conf. Ser.,* vol. 1436, J. Heerikhuisen et al., pp. 321–330, AIP, Melville, N. Y., doi:10.1063/1.4723626.

Pogorelov, N. V., S. N. Borovikov, L. F. Burlaga, R. W. Ebert, J. Heerikhuisen, T. K. Kim, I. A. Kryukov, S. T. Suess, S. T. Wu, and G. P. Zank (2012b), Numerical modeling of the solar wind flow with observational boundary conditions, in *Proceedings of the 11th Annual International Astrophysics Conference, Am. Inst. of Phys. Conf. Ser.,* vol. 1500, edited by Q. Hu et al., pp. 134–139, AIP, Melville, N. Y., doi:10.1063/1.4768756.

Pogorelov, N. V., S. N. Borovikov, M. C. Bedford, J. Heerikhuisen, T. K. Kim, I. A. Kryukov, and G. P. Zank (2013a), Modeling solar wind flow with the multi-scale fluid-kinetic simulation suite, in *Numerical Modeling of Space Plasma Flows (ASTRONUM2012), Astron. Soc. of the Pacific Conf. Ser.*, vol. 474, edited by N. V. Pogorelov, E. Audit, and G. P. Zank, p. 165, ASP, San Francisco, Calif.

Pogorelov, N. V., S. T. Suess, S. N. Borovikov, R. W. Ebert, D. J. McComas, and G. P. Zank (2013b), Three-dimensional features of the outer heliosphere due to coupling between the interstellar and interplanetary magnetic fields. IV. Solar cycle model based on Ulysses observations, *Astrophys. J.*, *772*, 2, doi:10.1088/0004-637X/772/1/2.

Richardson, I. G., and H. V. Cane (2010), Near-Earth interplanetary coronal mass ejections during solar cycle 23 (1996–2009): Catalog and summary of properties, *Sol. Phys.*, *264*, 189–237, doi:10.1007/s11207-010-9568-6.

Schwenn, R. (1990), *Large-Scale Structure of the Interplanetary Medium*, 99 pp., Springer, Berlin, Germany.

Sokół, J. M., M. Bzowski, M. Tokumaru, K. Fujiki, and D. J. McComas (2013), Heliolatitude and time variations of solar wind structure from in situ measurements and interplanetary scintillation observations, *Sol. Phys.*, *285*, 167–200, doi:10.1007/s11207-012-9993-9.

Tappin, S. J. (1987), Numerical modelling of scintillation variations from interplanetary disturbances, *Planet. Space Sci.*, *35*, 271–283, doi:10.1016/0032-0633(87)90153-X.

Tokumaru, M., M. Kojima, Y. Ishida, A. Yokobe, and T. Ohmi (2000a), Large-Scale structure of solar wind turbulence near solar activity minimum, *Adv. Space Res.*, *25*, 1943–1946, doi:10.1016/S0273-1177(99)00630-4.

Tokumaru, M., M. Kojima, K. Fujiki, and A. Yokobe (2000b), Three-dimensional propagation of interplanetary disturbances detected with radio scintillation measurements at 327 MHz, *J. Geophys. Res.*, *105*, 10,435–10,454, doi:10.1029/2000JA900001.

Tokumaru, M., M. Kojima, K. Fujiki, M. Yamashita, and A. Yokobe (2003a), Toroidal-shaped interplanetary disturbance associated with the halo coronal mass ejection event on 14 July 2000, *J. Geophys. Res.*, *108*, 1220, doi:10.1029/2002JA009574.

Tokumaru, M., M. Kojima, K. Fujiki, and M. Yamashita (2003b), Global structure of interplanetary coronal mass ejections retrieved from the model fitting analysis of radio scintillation observations, in *Solar Wind Ten, American Institute of Physics Conference Series,* vol. 679, edited by M. Velli et al., pp. 729–732, AIP, Melville, N. Y., doi:10.1063/1.1618696.

Tokumaru, M., M. Kojima, K. Fujiki, M. Yamashita, and D. Baba (2005), Interplanetary consequences caused by the extremely intense solar activity during October–November 2003, *J. Geophys. Res.*, *110*, A01109, doi:10.1029/2004JA010656.

Tokumaru, M., M. Kojima, K. Fujiki, and M. Yamashita (2006), Tracking heliospheric disturbances by interplanetary scintillation, *Nonlinear Processes Geophys.*, *13*, 329–338.

Tokumaru, M., M. Kojima, K. Fujiki, M. Yamashita, and B. V. Jackson (2007), The source and propagation of the interplanetary disturbance associated with the full-halo coronal mass ejection on 28 October 2003, *J. Geophys. Res.*, *112*, A05106, doi:10.1029/2006JA012043.

Tokumaru, M., M. Kojima, and K. Fujiki (2010), Solar cycle evolution of the solar wind speed distribution from 1985 to 2008, *J. Geophys. Res.*, *115*, A04102, doi:10.1029/2009JA014628.

Tokumaru, M., M. Kojima, K. Fujiki, K. Maruyama, Y. Maruyama, H. Ito, and T. Iju (2011), A newly developed UHF radiotelescope for interplanetary scintillation observations: Solar wind imaging facility, *Radio Sci.*, *46*, RS0F02, doi:10.1029/2011RS004694.

Tokumaru, M., M. Kojima, and K. Fujiki (2012), Long-term evolution in the global distribution of solar wind speed and density fluctuations during 1997–2009, *J. Geophys. Res.*, *117*, A06108, doi:10.1029/2011JA017379.

Watanabe, T., and T. Kakinuma (1972), The recurrent solar wind streams observed by interplanetary scintillation of 3C 48, *Publ. Astron. Soc. Jpn.*, *24*, 459.

Yu, H.-S., B. V. Jackson, P. P. Hick, A. Buffington, J. M. Clover, and M. Tokumaru (2012), 3-D reconstruction of the inner heliosphere from remote-sensing data: A global solar wind boundary that includes CME transient effects, in *American Institute of Physics Conference Series,* vol. 1500, edited by Q. Hu et al., pp. 147–152, AIP, Melville, N. Y., doi:10.1063/1.4768758.

Zhao, X., and J. T. Hoeksema (1995), Predicting the heliospheric magnetic field using the current sheet-source surface model, *Adv. Space Res.*, *16*, 181–184, doi:10.1016/0273-1177(95)00331-8.

Zhao, X. P., and J. T. Hoeksema (2010), The magnetic field at the inner boundary of the heliosphere around solar minimum, *Sol. Phys.*, *266*, 379–390, doi:10.1007/s11207-010-9618-0.